



45 eastern AP, meltwater ponding and associated fracturing was implicated in their rapid
46 disintegration through hydrofracture (e.g. Banwell et al., 2013; Scambos et al., 2000). In
47 contrast, at the Wordie and Wilkins ice shelves on the western AP, surface and /or subsurface
48 meltwater likely promoted the propagation of shallow surface crevasses into full-depth rifts, as
49 meltwater infilled crevassed areas (Doake et al., 1991; Scambos et al., 2009).

50

51 Given the evidence for meltwater-driven ice-shelf instability across the AP, renewed regional
52 warming (T_{2m}) since 2015, and projections of a non-linear increase in surface melt under future
53 warming (Gilbert and Kittel, 2021; Trusel et al., 2015), identifying recent changes in ice-shelf
54 surface meltwater regimes is essential. Two phenomena are of particular interest: (i)
55 meltwater-driven hydrofracture events and (ii) lateral surface meltwater export, either off the
56 ice-shelf edge or through rift systems. Whilst ice-shelf hydrofracture is increasingly
57 investigated through field-based (Banwell et al., 2024) and remotely-sensed observations
58 (Dunmire et al., 2020; Sommer et al., 2024.; Trusel et al., 2022), evidence for lateral surface
59 meltwater export remains scarce (Bell et al., 2017).

60

61 Here, we present evidence for the re-initiation of lateral surface meltwater export from the
62 Bach Ice Shelf after a 9-year hiatus. Using a combination of optical remote sensing and
63 regional climate model outputs, we document the return of this phenomenon and examine the
64 conditions that enabled it. We map cumulative summer (November–March) surface meltwater
65 areas across the ice shelf using a multi-band thresholding approach applied to Landsat 7, 8
66 and 9 records (2012–2025). To support these observations, we use a 43-year (1980–2023)
67 climatology comprising cumulative annual (April–March) gridded snowmelt and SMB products
68 from the Regional Atmospheric Climate Model (RACMO2 (Noël et al., 2023)). From these, we
69 derive the melt-to-SMB ratio as an indicator of surface ponding or runoff potential (a
70 conservative approach *adapted from* Donat-Magnin et al. (2021), van Wessem et al. (2023)
71 and Pfeffer et al. (1991)). These data are then complemented by mean annual (April–March)
72 T_{2m} data from ERA5 reanalysis for 1980–2025 (Hersbach et al., 2020), as the authors did not
73 have access to downscaled RACMO2 T_{2m} data at the time of writing.

74

75

76 **2. Methods**

77 2.1 Maximum Summer Surface Meltwater Extents

78 Maximum ice-shelf surface meltwater (i.e., water in lakes and streams) extents for each austral
79 summer (November–March) in the Landsat 8 and 9 record were mapped using an adapted
80 version of the multi-band thresholding approach (Moussavi et al., 2020). All available Landsat
81 8 and 9 Top-of-Atmosphere, Tier-2, Collection-2 images were classified using the thresholds
82 presented in Tuckett et al. (2025). To ensure data quality, each water mask was manually
83 cleaned by a subject expert. The cleaned masks for each melt season were then stacked to
84 produce a maximum surface meltwater extent for that summer.

85

86 In addition to the Landsat 8/9 summer products, a corresponding surface meltwater extent
87 was generated for the 2012/13 austral summer using Landsat 7 data alone. This season was



88 selected because it provides insight into the extent of surface ponding and run-off immediately
89 prior to the onset of the observed nine-year hiatus in lateral surface meltwater export.
90 Consistent image-selection criteria, multi-band thresholds, and manual masking procedures
91 were applied, following the same approach used for Landsat 8 and 9. For each austral summer
92 investigated, we visually examined the maximum ice-shelf surface meltwater extents, paying
93 particular attention to years in which surface meltwater features intersect with rifts and/or the
94 calving margin, as an indicator of surface meltwater runoff.

95

96 2.2 Rift Extents

97 Bach Ice Shelf's dominant, but still nascent, rift system (see Figure 1) was manually digitised
98 for each year in which summer surface meltwater extents were produced (2012/13–2024/25).
99 Image selection for rift digitisation focused on identifying the least cloudy scene available from
100 as late in the melt season as possible, to capture maximum rift extent. The final images used
101 (comprising a mix of Landsat 7, 8, and 9 Top-of-Atmosphere, Tier-2, Collection-2 scenes) are
102 given in Table S1. Rifts were digitised at a scale of 1:50,000 using only the red–green–blue
103 (RGB) band combination.

104

105 2.3 Modelled Melt and Surface Mass Balance

106 To quantify snowmelt and SMB over Bach Ice Shelf, we used the Regional Atmospheric
107 Climate Model (RACMO2.3p2), forced by ERA5 reanalysis, with daily 27 km × 27 km outputs
108 statistically downscaled to 2 km × 2 km resolution (Noël et al., 2023). We applied an ice-shelf
109 mask (Gerrish et al., 2024) to extract values over Bach Ice Shelf and calculated cumulative
110 snowmelt and SMB for each melt year, defined as April to March of the following year. By
111 defining the year as April to March we were able to capture the SMB and snowmelt conditions
112 preceding and spanning each full melt season, allowing us to consider the winter evolution of
113 the snow/firn layer.

114

115 2.4 Melt to Surface Mass Balance Ratio (Melt-to-SMB)

116 Melt-to-SMB ratios were derived from statistically downscaled (2 km) RACMO2.3p2 snowmelt
117 and SMB fields (Noël et al., 2023). While previous studies report melt-over-accumulation
118 (MOA) ratios (Donat-Magnin et al., 2021; Melchior Van Wesseem et al., 2023; Pfeffer et al.,
119 1991), commonly computed as liquid input (snowmelt + rainfall) relative to solid input (snowfall,
120 sometimes adjusted for sublimation; Esch et al., 2025), we use melt alone in the numerator
121 and SMB in the denominator for practical and conceptual reasons. Practically, we opted to
122 use the highest resolution dataset available as it likely better represents processes across
123 Bach Ice Shelf, even though separate rainfall and accumulation fields were not available.
124 Conceptually, SMB integrates the key processes that regulate firn air content, namely solid
125 and liquid precipitation, sublimation/evaporation, wind-driven snow redistribution, and runoff
126 (Lenaerts et al., 2019). Using a coarser resolution version of RACMO at 11 km with a wider
127 availability of SMB-relevant variables (van Dalum et al., 2024) indicates rainfall is generally
128 very small on Bach ice Shelf and including rain in the numerator and/or denominator would
129 shift ratios only slightly, and the main conclusions of our study would be unaffected.

130



131 **2.5 Modelled 2 m Air Temperatures (T_{2m})**

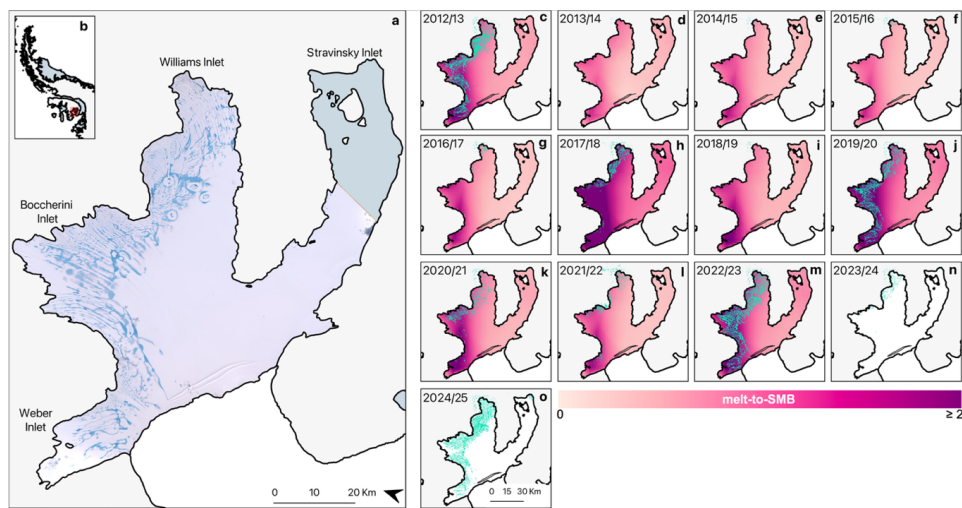
132 We used the European Centre for Medium-Range Weather Forecasts (ECMWF) Reanalysis
133 v5 (ERA5 (Hersbach et al., 2020)) to quantify mean annual 2 m air temperature (T_{2m}) over
134 Bach Ice Shelf. ERA5 provides hourly atmospheric reanalysis at $0.25^\circ \times 0.25^\circ$ grid spacing.
135 Using an ice-shelf mask from Gerrish et al. (2024) we extracted T_{2m} values over Bach Ice Shelf
136 and computed daily ice-shelf-averaged temperatures. Annual mean T_{2m} was then calculated
137 for each melt year (1980-2025), defined as April to March of the following year. By defining
138 the year as April-March, our T_{2m} data were consistent with our modelled snowmelt and SMB
139 data (Section 2.3).

140

141 **3. Results and Discussion**

142 Our results show renewed surface meltwater runoff from the calving margin beginning in the
143 2022/23 melt season, following nearly a decade of inactivity. During the hiatus, cumulative
144 summer surface meltwater areas across the ice shelf did not exceed 90 km^2 and surface
145 meltwater was typically clustered within Williams Inlet near the ice-shelf grounding line (Figs.
146 1, 2). The 2019/20 melt season was an exception, with lateral surface meltwater transport
147 across the ice-shelf surface but no clear evidence of surface meltwater export, and a
148 cumulative melt area of 236 km^2 . The hiatus ended in 2022/23, when surface meltwater was
149 not only extensive (329 km^2), but was exported via two main pathways: (i) over the ice-shelf
150 edge and (ii) into a nascent rift system (Fig. 1).

151



152

153 **Figure 1: Surface meltwater extent and melt-to-SMB ratio for the austral summers of 2012/13 to**
154 **2024/25. a)** Sentinel-2 image of Bach Ice Shelf on 08/02/2022, (b) places Bach Ice Shelf in the context
155 of the Antarctic Peninsula. (c - o) Cumulative surface meltwater extent (teal) and rift extent (black
156 polylines) for each austral summer (November–March), overlain on the mean annual melt-to-SMB ratio
157 derived from RACMO2.3p2 (Noël et al., 2023) (April preceding to March ending each melt season).
158 Darker pinks show high melt-to-SMB values, while lighter pinks represent relatively lower melt-to-SMB
159 values. Shapefile data from the SCAR Antarctic Digital Database, 2024 (Gerrish et al., 2024). Note for
160 2023/34 onwards melt-to-SMB values were unavailable.



161 Evaluating cumulative summer surface meltwater extent in the context of mean ice-shelf
162 integrated snowmelt and SMB reveals that the first four years of the nine-year hiatus
163 (2013/14–2016/17) correspond to periods when SMB markedly exceeded snowmelt (Fig. 2a).
164 As a consequence, average melt-to-SMB values fell below the thresholds previously used to
165 indicate surface ponding and run-off potential; 0.7 (Melchior Van Wessem et al., 2023; Pfeffer
166 et al., 1991) and 0.85 (Donat-Magnin et al., 2021) (Fig. 2b). In contrast, from 2017/18 onwards
167 the difference between snowmelt and SMB was reduced, and for two years (2017/18 and
168 2019/20) average snowmelt exceeded average SMB. As a result, melt-to-SMB values
169 exceeded 0.7 in all but one year from 2017/18 onward, consequently meeting the lower of the
170 previously established thresholds for ponding and runoff, and ranging between 0.75 and 1.35
171 (Fig. 2). This relatively sustained period of elevated melt-to-SMB values likely preconditioned
172 the ice shelf for widespread ponding events (e.g. the austral summers of 2019/20, 2022/23,
173 and 2024/25) and for the occurrence of lateral surface meltwater export, observed in 2022/23
174 and 2024/25 (Fig. 1).

175

176 From 1981 to 2025, mean annual T_{2m} (April - March) was marked by large year-to-year
177 variability, but a linear regression over the period indicates a trend of $+0.06^{\circ}\text{C yr}^{-1}$ ($p < 0.001$).
178 Temperatures were lowest in 1980/81 (-14.4°C) and highest in 2022/23 (-8.4°C) (Fig. 2), with
179 a 45-year annual mean of $-11.1 \pm 1.4^{\circ}\text{C}$. This overall warming trend is episodic. Temperatures
180 were remarkably stable between 2001/02 and 2005/06 ($-10.7 \pm 0.2^{\circ}\text{C}$), followed by a slight
181 but consistent decline from -10.6°C in 2003/04 to -11.8°C in 2006/07. Following this, T_{2m}
182 rebounded and warming became particularly pronounced in 2019/20, culminating in record
183 high temperatures in 2022/23 (-8.36°C).

184

185 Overall, our findings indicate that lateral surface meltwater export resumed on Bach Ice Shelf
186 in 2022/23, ending a nine-year hiatus beginning in 2013/14. The onset of this hiatus was likely
187 driven by a four-year interval during which SMB values were high relative to snowmelt (i.e.,
188 low melt-to-SMB ratios). During this period, firn-air content on the ice shelf likely increased,
189 enabling meltwater to percolate into and refill pore space rather than forming surface ponds
190 or driving lateral export (Kuipers Munneke et al., 2014). Although several subsequent years
191 exhibited high melt-to-SMB ratios (e.g. 2017/18), extensive surface ponding did not reappear
192 until 2019/20, and lateral surface meltwater export did not resume until 2022/23. This lag in
193 surface meltwater expression likely reflects a delayed system response, with the ice shelf
194 buffered by the firn-air reservoir generated during the preceding high-accumulation years.

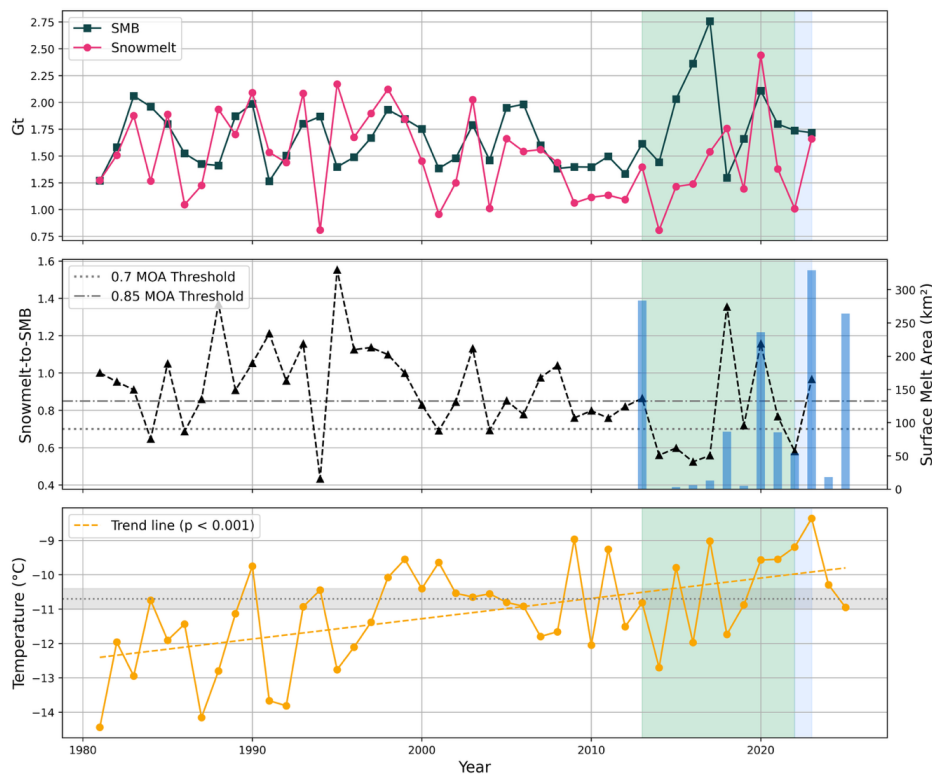
195

196 Previous studies have demonstrated clear links between T_{2m} and both accumulation and melt
197 on ice shelves, with surface melt increasing exponentially as T_{2m} rises and accumulation
198 responding more linearly (Gilbert and Kittel, 2021; Trusel et al., 2015). Here, our T_{2m} record
199 up to 2022/23 indicates that this melt season exhibits both the highest T_{2m} (-8.36°C) and the
200 greatest maximum surface meltwater extent on the ice shelf (329 km^2). Notably, this same
201 year also marks the return of lateral surface meltwater export. While T_{2m} remained relatively



202 consistent across the ice shelf between 2001/02 and 2005/06, we identify a significant long-
203 term warming trend of $+0.06 \text{ }^\circ\text{C yr}^{-1}$ ($p < 0.001$) over the 45-year climatology.

204



205 **Figure 2: Time series of mean annual (April-Mar) Surface Mass Balance, melt-to-SMB ratios, and**
206 **2m air temperatures.** (a) Surface Mass Balance and Snowmelt from RACMO2.3p2 (1980-2023) (2km
208 $\times 2\text{km}$) (Noël et al., 2023), (b) melt-to-SMB ratio, derived from RACMO2.3p2 (1980-2023) (2km \times 2km)
209 (Noël et al., 2023), and (c) 2m air temperatures from ERA5 (1980-2025) (Hersbach et al., 2020). Total
210 annual maximum surface meltwater area is also plotted on (b) for the period of 2012/13 – 2024/25, as
211 derived from Landsat 7, 8 and 9 optical imagery. The green shaded regions denote the 9-year hiatus in
212 surface meltwater export, and the blue shaded region marks the subsequent reactivation of lateral
213 surface meltwater export from the ice shelf. For all panels, x-axis tick marks denote April-March melt
214 seasons for RACMO2.3p2 and ERA5 data (e.g. 1981 = Apr 1980-Mar 1981), and November-March
215 seasons for total annual maximum lake areas. Additional grey dashed and dotted lines in (b) denote
216 two published MOA thresholds: 0.7 (Melchior Van Wessem et al., 2023; Pfeffer et al., 1991) and 0.85
217 (Donat-Magnin et al., 2021). The dashed and shaded line in (c) marks the T_{z_m} threshold of -10.7 ± 0.3
218 $^\circ\text{C}$, as calculated by (Melchior Van Wessem et al., 2023).
219

220 Given projected warming on the Antarctic Peninsula under a range of 21st-century climate
221 scenarios, it is increasingly pertinent to consider how Bach's surface meltwater network will
222 respond. In this context, our cumulative surface meltwater extents (Fig. 1) partially intersect



223 regions that are both vulnerable to hydrofracture and provide active buttressing, as identified
224 by Lai et al. (2020). Continued surface melting may therefore drive hydrofracture in these
225 regions and promote both ice-shelf weakening and broader ice-sheet instability.

226 **4. Concluding Remarks**

227 Ultimately, whether lateral surface meltwater export continues on Bach Ice Shelf depends on
228 the balance between snowmelt and accumulation, and therefore on future variations in T_{2m} .
229 The end of the nine-year hiatus in lateral surface meltwater export may indicate a transition
230 toward climatic conditions in which SMB no longer provides an effective buffer against surface
231 melt (Veldhuijsen et al., 1983). Moreover, while annual mean temperatures on the ice shelf
232 currently ensure that snowfall dominates the precipitation regime, further increases in T_{2m}
233 could lead to more frequent rain-on-snow events (Vignon et al., 2021). These events may
234 promote additional firn saturation and intensify surface meltwater expression, reinforcing the
235 positive melt–albedo feedback.

236 The consequences of increased ponding and/or lateral surface meltwater export on Bach Ice
237 Shelf are several-fold: meltwater ponds promote ice-shelf flexure and fracture and may drive
238 ice-shelf collapse in extreme cases. Further, a continuation of the observed lateral surface
239 meltwater export (i) off the ice-shelf edge, and (ii) into the nascent rift system has the potential
240 to drive ice-shelf thinning and promote ice-shelf calving events respectively. Given the
241 anticipated climate warming across Antarctica, the reactivation of lateral surface meltwater
242 export on Bach Ice Shelf may signal a shift toward conditions in which the buffering of
243 meltwater by accumulated snow is progressively overwhelmed, increasing the likelihood of
244 sustained meltwater export and reduced ice-shelf stability.



245 **Data Availability**

246 All data processing scripts as well as maximum summer surface meltwater extents and rift
247 extents will be made publicly available upon final publication via Github. ERA5 reanalysis is
248 publicly available through the Climate Data Store
249 (<https://cds.climate.copernicus.eu/datasets/reanalysis-era5-single-levels?tab=overview>).
250 Statistically downscaled RACMO2.3p2 products are freely available upon request to Brice
251 Noël (bnoel@uliege.be). The Bach Ice Shelf shapefile can be accessed at:
252 <https://doi.org/10.5285/4ecd795d-e038-412f-b430-251b33fc880e> (Gerrish et al., 2024).

253

254 **Author Contributions**

255 RLD, MLM, and LT conceptualised the study, conducted formal analysis. RLD lead original
256 draft preparation, supported by MLM. RLD conducted data visualisation. All authors
257 contributed to data curation and reviewed and edited the manuscript.

258

259 **Acknowledgements**

260 The authors thank Brice Noël, University of Liège, for providing download access to daily
261 RACMO2.3p2 products.

262

263 **Financial Support**

264 M. L. Maclennan is funded by the Natural Environment Research Council funded PICANTE
265 (Processes, Impacts and Changes of ANTArctic Extreme weather; Grant No. NE/Z503356/1)
266 project. R. L. Dell acknowledges support from a Royal Society Research Grant under grant
267 RGS\R2\242465. L. D. Trusel and M. Bahrami acknowledge support from NASA Cryospheric
268 Science Program grant 80NSSC24K1447 and NASA Future Investigators in NASA Earth And
269 Space Science and Technology Program grant 80NSSC24K1694.

270

271

272

273

274

275

276

277

278

279

280

281



282 **References**

283

284 Banwell, A. F., MacAyeal, D. R., and Sergienko, O. V.: Breakup of the Larsen B Ice Shelf
285 triggered by chain reaction drainage of supraglacial lakes, *Geophysical Research Letters*,
286 40, 5872–5876, <https://doi.org/10.1002/2013GL057694>, 2013.

287 Banwell, A.F., Willis, I.C., Stevens, L.A., Dell, R.L. and MacAyeal, D.R.: Observed
288 meltwater-induced flexure and fracture at a doline on George VI Ice Shelf,
289 Antarctica. *Journal of Glaciology*, 70, p.e47, 2024

290 Bell, R. E., Chu, W., Kingslake, J., Das, I., Tedesco, M., Tinto, K. J., Zappa, C. J., Frezzotti,
291 M., Boghosian, A., and Lee, W. S.: Antarctic ice shelf potentially stabilized by export of
292 meltwater in surface river, *Nature*, <https://doi.org/10.1038/nature22048>, 2017.

293 Carrasco, J.F., Bozkurt, D. and Cordero, R.R.: A review of the observed air temperature in
294 the Antarctic Peninsula. Did the warming trend come back after the early 21st hiatus?. *Polar*
295 *Science*, 28, p.100653, 2021

296 Cook, A.J. and Vaughan, D.G.: Overview of areal changes of the ice shelves on the
297 Antarctic Peninsula over the past 50 years. *The cryosphere*, 4(1), pp.77-98, 2010

298 Doake, C.S.M. and Vaughan, D.G.: Rapid disintegration of the Wordie Ice Shelf in response
299 to atmospheric warming. *Nature*, 350(6316), pp.328-330, 1991

300 Donat-Magnin, M., Jourdain, N.C., Kittel, C., Agosta, C., Amory, C., Gallée, H., Krinner, G.
301 and Chekki, M.: Future surface mass balance and surface melt in the Amundsen sector of
302 the West Antarctic Ice Sheet. *The Cryosphere*, 15(2), pp.571-593, 2021

303 Dunmire, D., Lenaerts, J.T.M., Banwell, A.F., Wever, N., Shragge, J., Lhermitte, S., Drews,
304 R., Pattyn, F., Hansen, J.S.S., Willis, I.C. and Miller, J.: Observations of buried lake drainage
305 on the Antarctic Ice Sheet. *Geophysical research letters*, 47(15), p.e2020GL087970, 2020

306 Esch, J., Van Den Broeke, M. and Van Tiggelen, M. Making the case for a two-step
307 evaluation of regional climate models: application to the melt-over-accumulation ratio in
308 Antarctica in RACMO2. 3p2. *Annals of Glaciology*, 66, p.e24, 2025

309 Fürst, J.J., Durand, G., Gillet-Chaulet, F., Tavard, L., Rankl, M., Braun, M. and Gagliardini,
310 O.: The safety band of Antarctic ice shelves. *Nature Climate Change*, 6(5), pp.479-482, 2016

311 Gerrish, L., Ireland, L., Fretwell, P., & Cooper, P: High resolution vector polygons of the
312 Antarctic coastline (Version 7.10) [Data set]. NERC EDS UK Polar Data Centre.
313 <https://doi.org/10.5285/4ecd795d-e038-412f-b430-251b33fc880e>, 2024

314 Gilbert, E. and Kittel, C.: Surface melt and runoff on Antarctic ice shelves at 1.5 C, 2 C, and
315 4 C of future warming. *Geophysical Research Letters*, 48(8), p.e2020GL091733, 2021

316 Hersbach, H., Bell, B., Berrisford, P., Hirahara, S., Horányi, A., Muñoz-Sabater, J., Nicolas,
317 J., Peubey, C., Radu, R., Schepers, D. and Simmons, A.: The ERA5 global
318 reanalysis. *Quarterly journal of the royal meteorological society*, 146(730), pp.1999-2049,
319 2020



- 320 Kittel, C., Amory, C., Agosta, C., Jourdain, N.C., Hofer, S., Delhasse, A., Doutreloup, S.,
321 Huot, P.V., Lang, C., Fichefet, T. and Fettweis, X.: Diverging future surface mass balance
322 between the Antarctic ice shelves and grounded ice sheet. *The Cryosphere*
323 *Discussions*, 2020, pp.1-29, 2020
- 324 Kuipers Munneke, P., Ligtenberg, S.R., Van Den Broeke, M.R. and Vaughan, D.G.: Firn air
325 depletion as a precursor of Antarctic ice-shelf collapse. *Journal of Glaciology*, 60(220),
326 pp.205-214, 2014
- 327 Lai, C.Y., Kingslake, J., Wearing, M.G., Chen, P.H.C., Gentine, P., Li, H., Spergel, J.J. and
328 van Wessem, J.M.: Vulnerability of Antarctica's ice shelves to meltwater-driven
329 fracture. *Nature*, 584(7822), pp.574-578, 2020
- 330 Lenaerts, J.T., Medley, B., van den Broeke, M.R. and Wouters, B.: Observing and modeling
331 ice sheet surface mass balance. *Reviews of Geophysics*, 57(2), pp.376-420, 2019
- 332 van Dalum, C., van de Berg, W. J., & van den Broeke, M. (2024). Monthly RACMO2.4p1
333 data for Antarctica (11 km) for SMB, SEB and near-surface variables (1979-2023) [Data set].
334 Zenodo. <https://doi.org/10.5281/zenodo.14217232>
- 335 van Wessem, J.M., van den Broeke, M.R., Wouters, B. and Lhermitte, S.: Variable
336 temperature thresholds of melt pond formation on Antarctic ice shelves. *Nature Climate*
337 *Change*, 13(2), pp.161-166, 2023
- 338 Moussavi, M., Pope, A., Halberstadt, A.R.W., Trusel, L.D., Cioffi, L. and Abdalati, W.:
339 Antarctic supraglacial lake detection using Landsat 8 and Sentinel-2 imagery: towards
340 continental generation of lake volumes. *Remote Sensing*, 12(1), p.134, 2020
- 341 Noël, B., Van Wessem, J.M., Wouters, B., Trusel, L., Lhermitte, S. and Van Den Broeke,
342 M.R.: Higher Antarctic ice sheet accumulation and surface melt rates revealed at 2 km
343 resolution. *Nature communications*, 14(1), p.7949, 2023
- 344 Pfeffer, W.T., Meier, M.F. and Illangasekare, T.H.: Retention of Greenland runoff by
345 refreezing: implications for projected future sea level change. *Journal of Geophysical*
346 *Research: Oceans*, 96(C12), pp.22117-22124, 1991
- 347 Scambos, T., Fricker, H.A., Liu, C.C., Bohlander, J., Fastook, J., Sargent, A., Massom, R.
348 and Wu, A.M.: Ice shelf disintegration by plate bending and hydro-fracture: Satellite
349 observations and model results of the 2008 Wilkins ice shelf break-ups. *Earth and Planetary*
350 *Science Letters*, 280(1-4), pp.51-60, 2009
- 351 Scambos, T.A., Hulbe, C., Fahnestock, M. and Bohlander, J.: The link between climate
352 warming and break-up of ice shelves in the Antarctic Peninsula. *Journal of*
353 *Glaciology*, 46(154), pp.516-530, 2000
- 354 Sommer, J., Izeboud, M., de Roda Husman, S., Wouters, B. and Lhermitte, S.: Brief
355 communication: Tides and damage as drivers of lake drainages on Shackleton Ice
356 Shelf. *The Cryosphere*, 19(11), pp.5903-5912, 2025



- 357 Trusel, L.D., Frey, K.E., Das, S.B., Karnauskas, K.B., Kuipers Munneke, P., Van Meijgaard,
358 E. and Van Den Broeke, M.R.: Divergent trajectories of Antarctic surface melt under two
359 twenty-first-century climate scenarios. *Nature Geoscience*, 8(12), pp.927-932, 2015
- 360 Trusel, L.D., Pan, Z. and Moussavi, M.: Repeated tidally induced hydrofracture of a
361 supraglacial lake at the Amery Ice Shelf grounding zone. *Geophysical Research*
362 *Letters*, 49(7), p.e2021GL095661, 2022
- 363 Tuckett, P.A., Sole, A.J., Livingstone, S.J., Jones, J.M., Lea, J.M. and Gilbert, E.: Continent-
364 wide mapping shows increasing sensitivity of East Antarctica to meltwater ponding. *Nature*
365 *Climate Change*, 15(7), pp.775-783, 2025
- 366 Turner, J., Colwell, S.R., Marshall, G.J., Lachlan-Cope, T.A., Carleton, A.M., Jones, P.D.,
367 Lagun, V., Reid, P.A. and Iagovkina, S.: Antarctic climate change during the last 50
368 years. *International journal of Climatology*, 25(3), pp.279-294, 2005
- 369 Turner, J., Lu, H., White, I., King, J.C., Phillips, T., Hosking, J.S., Bracegirdle, T.J., Marshall,
370 G.J., Mulvaney, R. and Deb, P.: Absence of 21st century warming on Antarctic Peninsula
371 consistent with natural variability. *Nature*, 535(7612), pp.411-415, 2016
- 372 Veldhuijsen, S., Van De Berg, W.J., Kuipers Munneke, P. and Van Den Broeke, M.R.: Firn
373 air content changes on Antarctic ice shelves under three future warming scenarios. *The*
374 *Cryosphere*, 18(4), pp.1983-1999, 2024
- 375 Vignon, É., Roussel, M.L., Gorodetskaya, I.V., Genthon, C. and Berne, A.: Present and future
376 of rainfall in Antarctica. *Geophysical Research Letters*, 48(8), p.e2020GL092281, 2021
377
378
379
380
381